14th International Symposium on Turbulence and Shear Flow Phenomena (TSFP14)
Heidelberg, Germany, July 28–31, 2026

MODELLING TURBULENCE WITH FRACTAL ENTANGLED VORTEX TUBES

Zishuo Han
State Key Laboratory for Turbulence and Complex Systems
School of Mechanics and Engineering Science, Peking University
Beijing 100871, China
zishuo_han@stu.pku.edu.cn

Weiyu Shen
Max Planck Institute for Solar System Research
Göttingen 37077, Germany
shenw@mps.mpg.de

Yue Yang
State Key Laboratory for Turbulence and Complex Systems
School of Mechanics and Engineering Science, Peking University
Beijing 100871, China
yyg@pku.edu.cn

ABSTRACT

We model turbulence using coherent vortices distributed within a multi-scale statistical framework, termed 'woven turbulence'. These entangled vortices are generated based on fractional Brownian bridges, with scale-dependent parameters set by dimensional analysis and geometric similarity. The spatial filling fraction of vortices in woven turbulence, termed 'vortex density', is tunable, enabling us to investigate the statistical-structural interaction and uncover two key physical insights of turbulence. First, the invariance of the hierarchical vortex density across scales corresponds to Kolmogorov's $-5/3$ law in the inertial range. Second, there exists a critical total vortex density at which the intermittency of woven turbulence closely matches that of real turbulence, and this critical density converges to a finite value in the inviscid limit. In addition, woven turbulence also serves as a fast turbulence synthesis method, requiring only the Taylor-Reynolds number as input and exhibiting an extremely low computational cost proportional to the grid size.

INTRODUCTION

Turbulence, prevalent in both natural and engineering contexts, is acknowledged as one of the most representative complex systems (Benzi & Toschi, 2023). The intricate physical mechanisms and the efficient simulation of turbulence remain significant challenges. Various turbulence modeling methods (e.g. Fung *et al.*, 1992; Patruno & Ricci, 2018; Zhou *et al.*, 2015) have been proposed to understand and synthesize turbulence.

Statistical modeling methods incorporate randomness and aim to reproduce turbulent statistics. For example, random Fourier modes (RFM) method (Patruno & Ricci, 2018) generates Fourier modes constrained by a specified energy spectrum so that it can reproduce low-order statistical features of turbulence. Fractal models are based on the concept of energy cascade and characterize turbulence as multi-scale self-similar vortices. These models, including monofractal models, e.g., the β-model (Frisch *et al.*, 1978), and multifractal models, e.g., the p-model (Meneveau & Sreenivasan, 1987), can reproduce high-order statistics of turbulence. Vortices in fractal models are either conceptual entities, or synthesized using mathematical tools like wavelet-based methods (Zhou *et al.*, 2015). However, vortices in turbulence are governed by complex dynamics, leading to intricate coherent structures that cannot be reproduced by current fractal models.

Coherent vortices are considered the key to understanding the physical mechanisms of turbulence (Pullin & Saffman, 1998; Yang *et al.*, 2023), as they govern energy transfer and dissipation. Structural modeling methods study possible flow structures in turbulence starting from the dynamics of the Navier-Stokes (NS) equations (Pullin & Saffman, 1998), offering a physics-based alternative pathway to turbulence modeling. Several vortex models, such as spherical, tubular, sheet, and spiral vortices, have been proposed to describe the fine-scale structures of turbulence. Given that vortices in real turbulence exhibit complex, intertwined coherent structures (She *et al.*, 1990), a critical issue lies in how to intricately assemble the fine-scale elements from these vortex models into a turbulent field.

Shen *et al.* (2024) proposed a bottom-up approach to model turbulence by linking Burgers vortices through quantum vortex filaments. This method simultaneously reproduces the intertwined coherent vortices, key statistics such as Kolmogorov's -5/3 law, and intermittency observed in real turbulence. However, in this approach, the thickness of vortex tubes varies only within a narrow range, and the overall multi-scale characteristics largely depend on the quantum vortex filaments. This limits the accurate reproduction of multi-scale features of turbulence and results in low computational efficiency.

Building upon the work of Shen *et al.* (2024) and incorporating a statistical fractal framework, this study models turbulence as stochastic fractal vortex tubes with a specific vortex density. The stochasticity is achieved by generating the vortex tube centerline using a fractional Brownian bridge (FBB), which is a computationally efficient stochastic process with adjustable multi-scale features (Friedrich *et al.*, 2020). We refer to the generated flow field as 'woven turbulence'. It generates vortex tubes that resemble real turbulence and reflect fluid dynamics, with inherent intermittency that is intuitively adjustable via the vortex density, and incorporates multi-scale characteristics and stochasticity from the statistical framework.

METHODS

The construction procedure of woven turbulence is sketched in Fig. 1. The woven homogeneous isotropic turbulence (HIT) is composed of multiple sets of stochastic vortices across $\mathcal{N}$ discrete scale levels within a periodic box V of side $\mathscr{L} = 2\pi$.

As shown in Fig. 1(a), each vortex tube is constructed along its curved centerline C, which is generated based on FBB discrete points $\boldsymbol{B}(J)$ in 3D space with index $J = 1, 2, ..., \mathscr{N}$. FBB exhibits Gaussianity and fractal behavior, with precise control over long-range correlations characterized by the scaling of the mean-squared distance (Friedrich *et al.*, 2020)

$$\langle(\boldsymbol{B}(J) - \boldsymbol{B}(J'))^2\rangle_{\mathscr{N}} = \delta_B^2 |J - J'|^{2H}, \tag{1}$$

where H denotes the Hurst exponent, $\langle\cdot\rangle_{\mathscr{N}}$ the average over $\mathscr{N}$ points and δ_B the FBB scale factor. For each vortex tube with core size σ characterizing its scale, we set the FBB scale $\delta_B = 40\sigma_i$. Note that the FBB is end-to-end connected in this work to ensure the closure of the vortex tube. Next, these discrete points of FBB are interpolated by the fifth-order splines and mapped into the periodic box V by taking the modulo with respect to the box side length $\mathscr{L}$. Then we obtain the vortex centerline C (shown as the blue dashed-dot line in Fig. 1(a)) with position $\boldsymbol{c}(s)$ along arc-length s. The length of centerline $L \approx c_H \delta_B \mathscr{N}$ is proportional to $\mathscr{N}$ and δ_B, where the value of the coefficient c_H is determined by H.

Subsequently, the vortex tube is generated based on its centerline C. The curved cylindrical coordinate system (s, ρ, θ) is introduced with the local cylindrical frame $(\boldsymbol{e}_s, \boldsymbol{e}_\rho, \boldsymbol{e}_\theta)$ in a tubular region surrounding centerline C with radius $\mathcal{R}$. The system satisfies $\boldsymbol{x}(s, \rho, \theta) = \boldsymbol{c}(s) + \rho\boldsymbol{e}_\rho(\theta)$. At the scale level with index $i \in \{1, 2, \ldots, \mathcal{N}\}$, the vorticity of the j-th vortex tube is specified by (Shen *et al.*, 2024)

$$\begin{aligned}&\boldsymbol{\omega}_T(\boldsymbol{x}(s,\rho,\theta)|\Gamma,\sigma,\boldsymbol{c}(s))\\ &= \Gamma G(s,\rho)\left[\boldsymbol{e}_s + \frac{\rho}{R(s)(1-\kappa(s)\rho\cos\theta)}\frac{\mathrm{d}R(s)}{\mathrm{d}s}\boldsymbol{e}_\rho\right],\end{aligned} \tag{2}$$

with the circulation Γ, the curvature κ, the Gaussian kernel function

$$G(s,\rho) = \begin{cases}\frac{1}{2\pi R(s)^2}\exp\left[\frac{-\rho^2}{2R(s)^2}\right], & \rho \in [0, \mathcal{R}),\\ 0, \quad \rho \in [\mathcal{R}, +\infty)\end{cases} \tag{3}$$

as in the vortex model of Burgers (1948), and the local vortex core size

$$R(s) = \sigma\left(1 + \lambda_\sigma\left(1 + \sin(2\pi M s/L)\right)\right). \tag{4}$$

Here, the core size σ represents the characteristic scale of the vortex tube, $\lambda_\sigma \geq 0$ denotes the core size variation magnitude and M the variation frequency.

The vorticity of woven turbulence $\boldsymbol{\omega} = \sum_{i=1}^{\mathcal{N}} \sum_{j=1}^{n_i} \boldsymbol{\omega}_{ij}$ is given by the sum of vorticity over all vortex tubes, where n_i denotes the population of vortex tubes at the i-th scale level, and the vorticity of the j-th vortex tubes at the i-th scale level is set as $\boldsymbol{\omega}_{ij}(\boldsymbol{x}) = \boldsymbol{\omega}_T(\boldsymbol{x}(s,\rho,\theta)|\Gamma_i, \sigma_i, \boldsymbol{c}_{ij}(s))$. The core size σ_i, centerline length L_i, population n_i, and circulation Γ_i of vortex tubes at different scales are set to satisfy self-similar relations

$$\begin{cases}\sigma_{i+1}/\sigma_i = r_\sigma,\\ L_{i+1}/L_i = r_L,\\ n_{i+1}/n_i = r_n,\\ \Gamma_{i+1}/\Gamma_i = r_\Gamma\end{cases} \tag{5}$$

for $i \in \{1, 2, \ldots, \mathcal{N} - 1\}$, where r_σ denotes the core size ratio, r_L the centerline length ratio, r_n the population ratio, and r_Γ the circulation ratio. In addition, the core size variation frequency $M_i = \lfloor 2L_i/\mathscr{L}\rceil / r_\sigma^{i-1}$ in Eq. (4) is set to ensure the similarity among vortex structures at different scales, where $\lfloor\cdot\rceil$ denotes the rounding operation. Generally, we set $r_\sigma = 1/2$ and $n_1 = 1$ as in typical fractal models (Frisch *et al.*, 1978; Meneveau & Sreenivasan, 1987).

Dimensional analysis suggests $\Gamma_i \sim \sigma_i^{4/3}$, so we set $r_\Gamma = r_\sigma^{4/3} = (1/2)^{4/3}$. This ratio is consistent with the DNS results (Iyer *et al.*, 2019). The length of the vortex tubes scales proportionally with their core size (Ghira *et al.*, 2022), yielding $r_L = r_\sigma = 1/2$. To quantify how much physical space the vortices occupy, we introduce the total vortex density $\varrho = \sum_{i=1}^{\mathcal{N}} \varrho_i$ with the hierarchical vortex density

$$\varrho_i = \frac{n_i L_i \sigma_i^2}{\mathscr{L}^3} = \frac{n_1 L_1 \sigma_1^2}{\mathscr{L}^3}(r_n r_L r_\sigma^2)^{i-1} \tag{6}$$

characterizing the abundance of vortices at the i-th scale level.

The specific settings of woven turbulence cases in this study are provided in Table 1. Note that the code of construction algorithm is available at `https://github.com/YYgroup/FastWeavTurb`.

RESULTS

The multi-scale self-similar vortices give rise to the inertial range in woven turbulence At each scale, we define the hierarchical energy spectrum $E_i(k) = \oint_{S(k)} \frac{1}{2}\hat{\boldsymbol{u}}_i(\boldsymbol{k})\overline{\hat{\boldsymbol{u}}}_i(\boldsymbol{k})\mathrm{d}S(k)$, where $\hat{\boldsymbol{u}}_i(\boldsymbol{k})$ denotes the velocity at the i-th scale level in Fourier space, $S(k)$ the sphere with a radius of k in Fourier

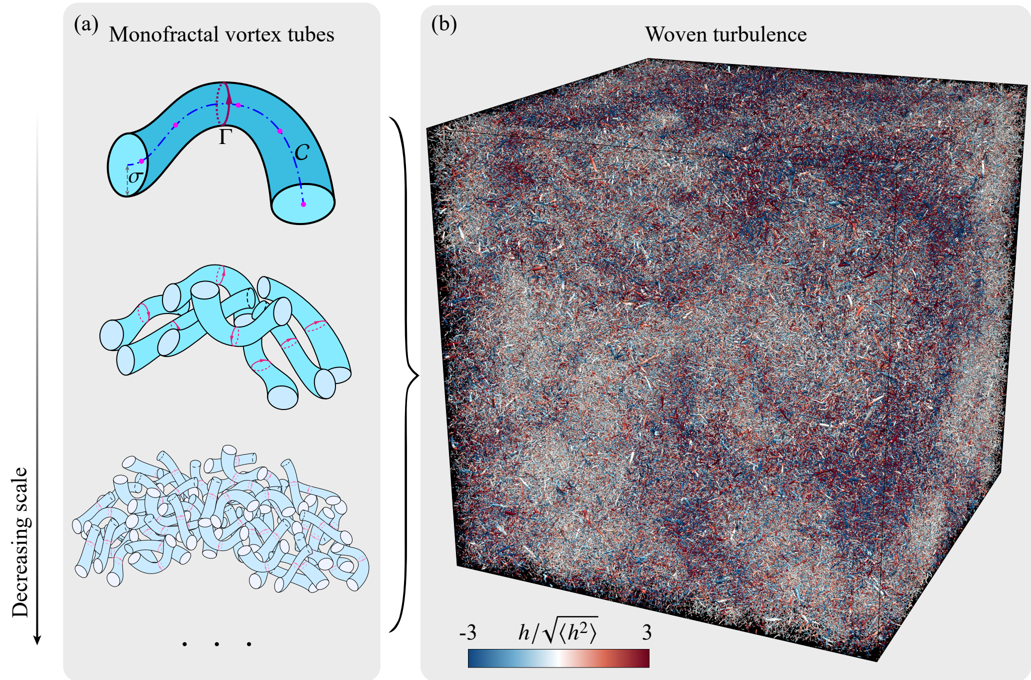

Figure 1. Construction of woven turbulence. (a) Schematic of multi-scale vortex tubes constituting woven turbulence. At the first scale level, we annotate the core size σ, the circulation Γ, and the centerline C of the vortex tube, with the underlying FBB discrete points $\boldsymbol{B}(J)$ indicated as purple points. Note that the vortex tubes are sketched as segments, but the actual ones in woven turbulence are closed. (b) Visualization of the woven turbulence case WT6 (with 4096^3 grid points and $Re_\lambda = 1237$, see Table 1). Flow fields in a $1/2^3$ spatial portion are visualized by isosurfaces of the vorticity magnitude $|\boldsymbol{\omega}| = 3\sqrt{\langle\Omega\rangle}$, where $\Omega = |\boldsymbol{\omega}|^2/2$ denotes the enstrophy and $\langle\cdot\rangle$ represents the volume average over the computational domain V. These isosurfaces are color-coded by the normalized helicity density $h/\sqrt{\langle h^2\rangle}$ with helicity density $h = \boldsymbol{u}\cdot\boldsymbol{\omega}$, where $\boldsymbol{u}$ and $\boldsymbol{\omega}$ denote the velocity and the vorticity, respectively.

Table 1. Setup of woven turbulence cases with Taylor-Reynolds numbers Re_λ from $O(10^2)$ to $O(10^3)$. All cases are normalized such that the root-mean-square velocity $u' = 1$.

Case	$\mathcal{N}$	$\sigma_\mathcal{N}$	Re_λ	ϱ	N
WT1	2	3.68×10^{-2}	101	3.40×10^{-2}	128
WT2	3	1.51×10^{-2}	159	2.40×10^{-2}	256
WT3	4	7.80×10^{-3}	268	1.70×10^{-2}	512
WT4	5	3.57×10^{-3}	419	1.28×10^{-2}	1024
WT5	6	1.70×10^{-3}	722	1.21×10^{-2}	2048
WT6	7	8.47×10^{-4}	1237	1.20×10^{-2}	4096

space, $\boldsymbol{k}$ the wavevector, $k = |\boldsymbol{k}|$ the wavenumber, and the overline represents the complex conjugate. Figure 2 plots the total and hierarchical energy spectra for case WT6, where the hierarchical spectra at different scales exhibit a similar shape. Since $E_i(k)$ spans a range of wavenumbers, for simplicity, we extract a representative value for each scale by introducing a characteristic energy $E_i(k_i)$, where $k_i = 1/(3\sigma_i)$ denotes the corresponding characteristic wavenumber. In Fig. 2, $E_i(k_i)$ and $E(k)$ both follow a $k^{-5/3}$ scaling in the inertial range. This agreement suggests the *hierarchical energy hypothesis*

$$\frac{E(k_{i+1})}{E(k_i)} = \frac{E_{i+1}(k_{i+1})}{E_i(k_i)}, \tag{7}$$

i.e., the scaling of $E(k)$ in woven turbulence can be captured through the ratio of hierarchical energies at adjacent scale levels. Based on the explicit vorticity expression Eq. (2), a quantitative relation between characteristic energy and vortex tube parameters is obtained as $E_i(k_i) \propto \Gamma_i^2 L_i n_i \sigma_i$. Substituting it into Eq. (7) with Eq. (5) yields the scaling exponent

$$r_I = -1 - \frac{\ln(r_n r_L) + 2\ln(r_\Gamma)}{\ln(r_\sigma)} \tag{8}$$

in inertial-range spectrum $E(k) \sim k^{r_I}$. We restrict the inertial-range wavenumbers $k \in [k_1, k_\mathcal{N}]$ to lie between the smallest and largest characteristic wavenumbers of multi-scale vortices. Substituting the core size ratio $r_\sigma = 1/2$, the centerline length ratio $r_L = 1/2$, and the circulation ratio $r_\Gamma = (1/2)^{4/3}$ into Eq. (8), we obtain Kolmogorov's -5/3 law $r_I = -5/3$ suggests $r_n = 8$ in woven turbulence. This value $r_n = 8$ corresponds to the scale invariance of the hierarchical vortex density $\varrho_i = \varrho/\mathcal{N}$ based on Eq. (6), which implies a self-similar spatial distribution of vortices across scales.

Derived from Eqs. (1) and (2), the spectrum in the energy-containing range satisfies $E(k) \sim k^{r_E}$ with the scaling exponent $r_E = 1/H - 2$. Thus, the role of H in controlling the spatial arrangement of vortex centerlines and thereby shaping the energy spectrum in this range is analogous to that of external forcing in real turbulence. Here we set $H = 5/6$, corresponding to $r_E = -4/5$, which is consistent with the scaling in Shen *et al.* (2024). In addition, numerical tests show that the decay behavior of dissipation range spectrum depends on the value of λ_σ in Eq. (4). When $\lambda_\sigma = 3/2$, the dissipation range spectrum approach exponential decay.

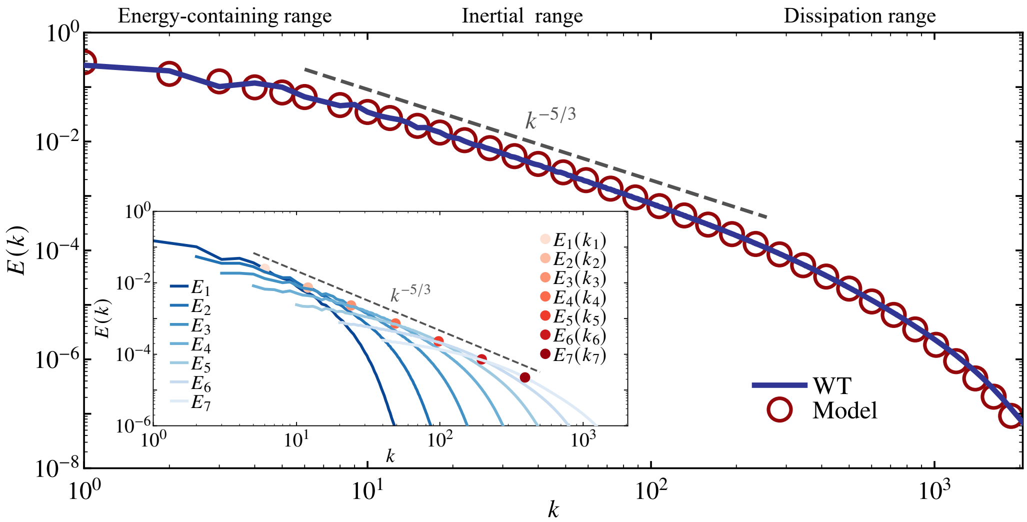

Figure 2. Energy spectrum $E(k)$ of case WT6 (see Table 1) with $Re_\lambda = 1237$ and the corresponding model spectrum in Eq. (11). The inset plots the hierarchical energy spectra $E_i(k)$ of case WT6 and the corresponding characteristic energy $E_i(k_i)$. Each hierarchical energy spectrum is shown around its characteristic wavenumber k_i, within the range $[k_i/10, 10k_i]$.

Similar to real turbulence, the wavenumber ranges of the three-regime energy spectrum are determined by characteristic length scales of vortices in woven turbulence. By matching the energy spectra of woven turbulence and real turbulence across a range of Re_λ from $O(10^2)$ to $O(10^3)$, we establish scale relations for the integral and Kolmogorov scales

$$\mathcal{L} = c_{\mathcal{L}}\sigma_1 \quad \text{and} \quad \eta = c_\eta \sigma_N, \tag{9}$$

respectively. Here, σ_1 and σ_N are the core sizes of the largest and smallest vortices, respectively, and the coefficients $c_{\mathcal{L}} = 20$ and $c_\eta = 0.59$ are calibrated from this spectral agreement. This intrinsic correspondence between vortex scales and turbulence statistical scales in Eq. (9) is independent of Re_λ (Ghira *et al.*, 2022). Considering the Kolmogorov length scale $\eta = (\nu^3/\langle\varepsilon\rangle)^{1/4}$ and the mean dissipation rate $\langle\varepsilon\rangle = 2\nu\langle\Omega\rangle$, the effective kinematic viscosity in woven turbulence is estimated by $\nu = \eta^2\sqrt{2\langle\Omega\rangle}$. With Eq. (9), the Taylor-Reynolds number reads

$$Re_\lambda = \frac{u'\lambda_T}{\nu} = \frac{\sqrt{15}(u')^2}{2\eta^2\langle\Omega\rangle} = \frac{\sqrt{15}(u')^2}{2(c_\eta\sigma_N)^2\langle\Omega\rangle}, \tag{10}$$

where $\lambda_T = u'\sqrt{15/(2\langle\Omega\rangle)}$ denotes the Taylor micro-scale, $u' = \sqrt{2E_t/3}$ the root-mean-square velocity, and $E_t = \int E(k)\mathrm{d}k$ the total kinetic energy. The normalized mean enstrophy $\langle\Omega\rangle/(u')^2 = \int k^2E(k)\mathrm{d}k/(u')^2$ is determined by the scale range from σ_1 to σ_N, since the scale range fully specifies the normalized energy spectrum $E(k)/(u')^2$. Thus, woven turbulence can be constructed for a specified Re_λ through determining the scale range from σ_1 to σ_N.

The model spectrum of turbulence (Pope, 2000), as an excellent fit to various turbulence data, is specified by

$$E(k) = C_E\left(\frac{k\mathcal{L}}{\left[(k\mathcal{L})^2+75\right]^{1/2}}\right)^{r_E-r_I} k^{r_I}\exp(-4.7k\eta), \tag{11}$$

with $r_E = -4/5$, $r_I = -5/3$, and the constant C_E determined by the total kinetic energy E_t. It is used to assess the spectrum of woven turbulence. For example, the spectrum of woven turbulence with $Re_\lambda = 1237$ agrees with the model spectrum in Fig. 2, with smooth transitions between the three wavenumber ranges. This agreement confirms that the three-regime energy spectrum is faithfully reproduced in woven turbulence.

In woven turbulence, intermittency arises from coherent vortex tubes and depends on the vortex density ϱ. As ϱ increases, as illustrated in Fig. 3, the woven turbulence transitions from a state of vortex clustering with strong intermittency to an approximately Gaussian random field without intermittency, and the energy spectrum remains unchanged.

Intermittency in turbulence is usually quantified by the deviation of the inertial-range scaling exponents ζ_p of p-th order structure functions $S_p(r) \sim r^{\zeta_p}$ from the K41 linear model $\zeta_p = p/3$. Note that the structure functions are defined as $S_p(r) = \langle[(\boldsymbol{u}(\boldsymbol{x}+r\boldsymbol{e}_m) - \boldsymbol{u}(\boldsymbol{x}))\cdot\boldsymbol{e}_m]^p\rangle$, where $\boldsymbol{e}_m$ is an arbitrary unit vector. We find that for each Taylor-Reynolds number Re_λ, there exists a critical vortex density ϱ such that ζ_p conform to those of DNS as shown in Fig. 4. In Fig. 5, the critical vortex density, fitted by

$$\varrho_c = 0.07\exp(-Re_\lambda/100) + 0.012, \tag{12}$$

decreases with Re_λ and tends to a finite value for large Re_λ. At the critical vortex density, woven turbulence simultaneously exhibits physically realistic vortex structures (see Fig. 6), Gaussian velocity distributions, and intermittency comparable to real turbulence. In addition, the difference in the scaling of the longitudinal and transverse structure functions, as well as the asymmetry of the local vorticity-strain correlation, is captured (not shown).

The construction of vortex tubes in woven turbulence is performed within the local tubular space along their centerlines, and thus the computational cost scales as $O(\varrho_c N^3)$. Since ϱ_c approaches a constant at high Reynolds numbers in Eq. (12), the effective scaling is $O(N^3)$, which is the optimal scaling for 3D turbulence synthesis. In contrast, the computational cost of the RFM is $O(N^3 \log N)$ (Fung *et al.*, 1992), consistent with that of the 3D fast Fourier transform. Figure 7 compares the computational costs of generating an instantaneous turbulent flow field using DNS, woven turbulence, and

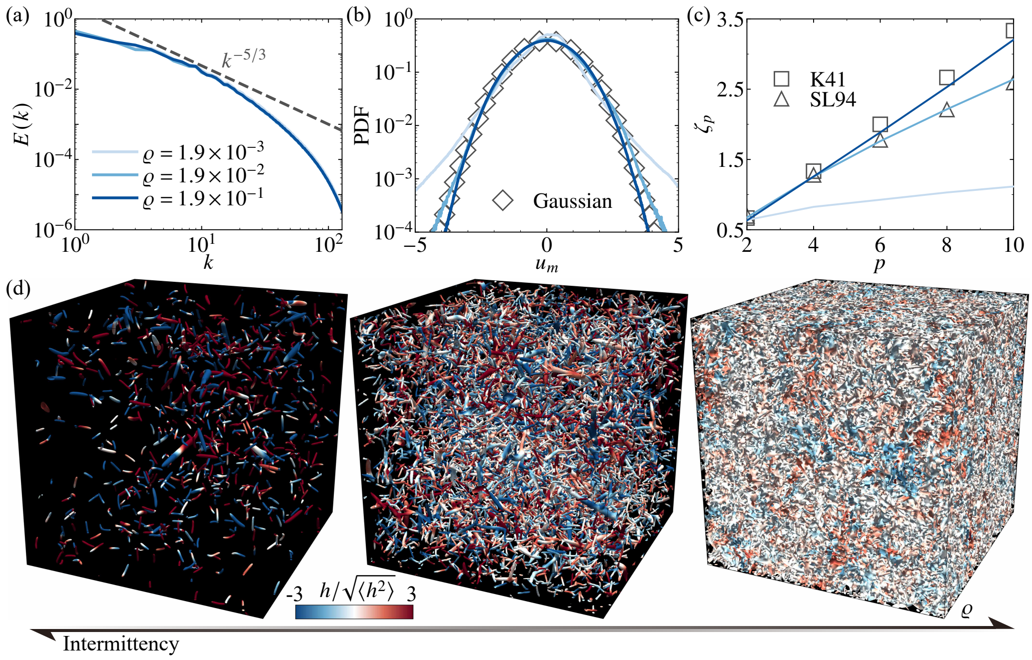

Figure 3. Effect of vortex density ϱ on the intermittency of woven turbulence with $Re_\lambda = 161$. The cases here include WT2 ($\varrho = 1.9 \times 10^{-2}$) in Table 1 and its variable-density counterparts ($\varrho = 1.9 \times 10^{-3}$ and 1.9×10^{-1}). (a) Energy spectra. (b) Probability density function (PDF) of velocity components u_m. (c) Scaling exponents of even-order structure functions, compared with K41 model $\zeta_p = p/3$ and SL94 model $\zeta_p = p/9 + 2[1-(2/3)^{p/3}]$ (She & Leveque, 1994). (d) Isosurfaces of vorticity magnitude $|\boldsymbol{\omega}| = \Gamma_1/(4\pi\sigma_1^2)$ color-coded by the normalized helicity density $h/\sqrt{\langle h^2 \rangle}$, with $\varrho = 1.9 \times 10^{-3}$,$1.9 \times 10^{-2}$, and 1.9×10^{-1} from left to right.

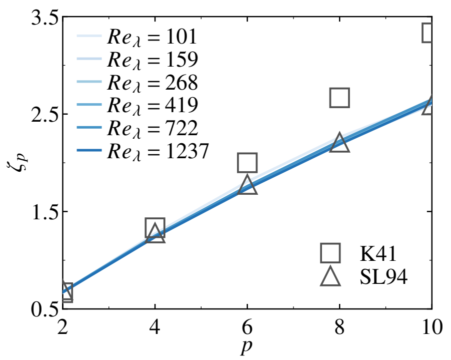

Figure 4. Scaling exponents ζ_p of even-order structure functions of woven turbulence with varying Re_λ, compared with K41 and SL94 model predictions.

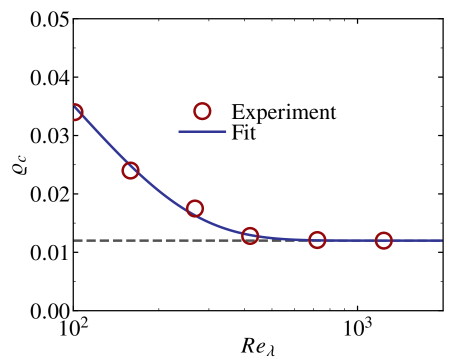

Figure 5. Critical vortex density ϱ_c of woven turbulence with varying Re_λ.

RFM at various Re_λ. The DNS cost is the computational time to evolve from the initial RFM field to a stationary turbulent state. These simulations were performed on the TianheXY-C at the National Supercomputer Center in Guangzhou, China. For $Re_\lambda > 200$, the computational cost of woven turbulence is less than 10^{-5} of that of DNS, and this difference becomes more significant as Re_λ increases. Moreover, although the cost of RFM is lower, the gap with woven turbulence narrows as Re_λ increases. Therefore, our method exhibits high computational efficiency in generating instantaneous turbulent fields.

In summary, we model turbulence using stochastic fractal entangled vortex tubes, combining the strengths of structural and statistical modelling. The method successfully reproduces key turbulence features, including the three-regime energy spectrum, intermittency, and coherent structures. It enables fast turbulence synthesis with optimal $O(N^3)$ computational scaling and only the Taylor-Reynolds number as input. Future work will explore vortex interactions and multifractal architectures to make woven turbulence closer to real turbulence.

REFERENCES

Benzi, R. & Toschi, F. 2023 Lectures on turbulence. *Phys. Rep.* **1021**, 1–106.

Burgers, J. M. 1948 A mathematical model illustrating the theory of turbulence. *Adv. Appl. Mech.* **1**, 171–199.

Friedrich, J., Gallon, S., Pumir, A. & Grauer, R. 2020 Stochastic interpolation of sparsely sampled time series via multipoint fractional Brownian bridges. *Phys. Rev. Lett.* **125**, 170602.

Frisch, U., Sulem, P.-L. & Nelkin, M. 1978 A simple dynamical model of intermittent fully developed turbulence. *J. Fluid Mech.* **87**, 719–736.

Fung, J. C. H., Hunt, J. C. R., Malik, N. A. & Perkins, R. J.

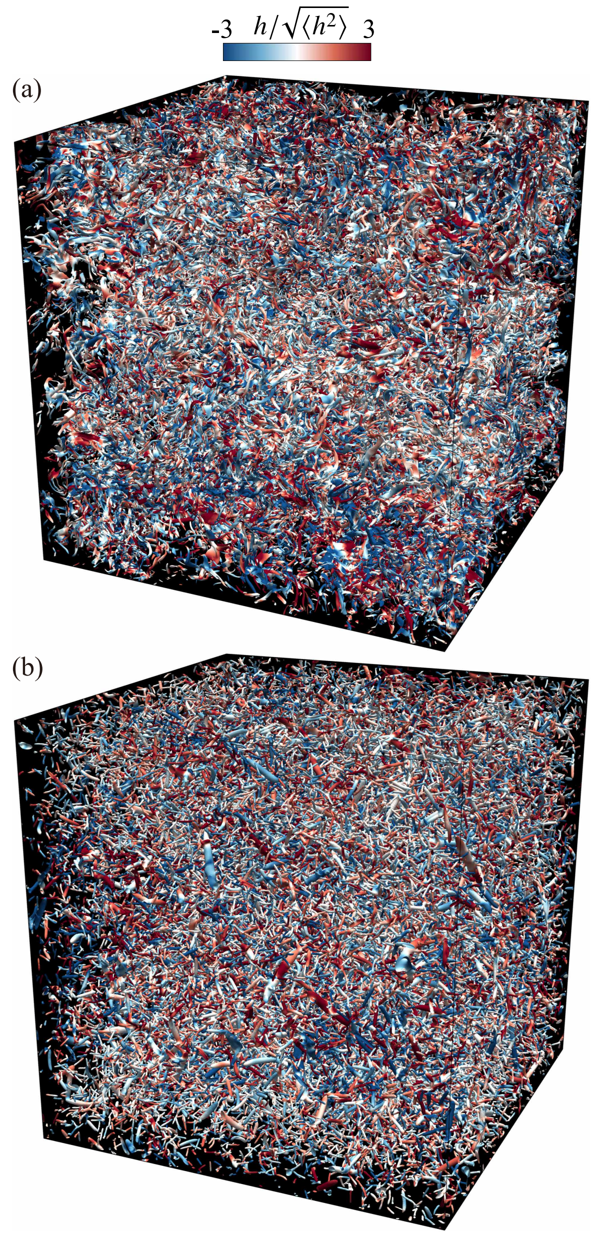

Figure 6. Isosurfaces of $|\boldsymbol{\omega}| = 3\sqrt{\langle \Omega \rangle}$ for (a) DNS case with $Re_\lambda = 261$ and the computational cost 1.0×10^4 CPU hours and (b) woven turbulence case WT3 with $Re_\lambda = 268$ and the computational cost 2.9×10^{-2} CPU hours. These isosurfaces are color-coded by $h/\sqrt{\langle h^2 \rangle}$.

1992 Kinematic simulation of homogeneous turbulence by unsteady random Fourier modes. *J. Fluid Mech.* **236**, 281–318.

Ghira, A. A., Elsinga, G. E. & da Silva, C. B. 2022 Characteristics of the intense vorticity structures in isotropic turbulence at high reynolds numbers. *Phys. Rev. Fluids* **7**, 104605.

Iyer, K. P., Sreenivasan, K. R. & Yeung, P. K. 2019 Circulation in high Reynolds number isotropic turbulence is a bifractal. *Phys. Rev. X* **9**, 041006.

Meneveau, C. & Sreenivasan, K. R. 1987 Simple multifractal cascade model for fully developed turbulence. *Phys. Rev. Lett.* **59**, 1424–1427.

Patruno, L. & Ricci, M. 2018 A systematic approach to the generation of synthetic turbulence using spectral methods.

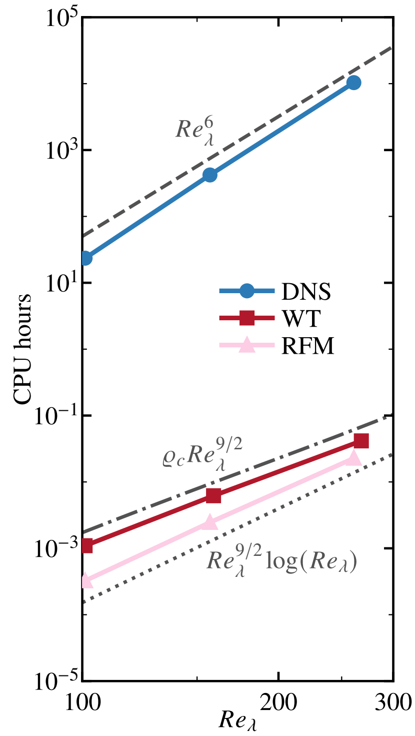

Figure 7. Computational costs of woven turbulence, DNS and RFM cases with varying Re_λ. Here, the energy spectra of the RFM are set to be the same as those of DNS at the same Re_λ These simulations were performed on the TianheXY-C at the National Supercomputer Center in Guangzhou, China.

Comput. Meth. Appl. Mech. Eng. **340**, 881–904.

Pope, S. B. 2000 *Turbulent Flows*. Cambridge: Cambridge University Press.

Pullin, D. I. & Saffman, P. G. 1998 Vortex dynamics in turbulence. *Annu. Rev. Fluid Mech.* **30**, 31–51.

She, Z.-S., Jackson, E. & Orszag, S. A. 1990 Intermittent vortex structures in homogeneous isotropic turbulence. *Nature* **344**, 226–228.

She, Z.-S. & Leveque, E. 1994 Universal scaling laws in fully developed turbulence. *Phys. Rev. Lett.* **72**, 336–339.

Shen, W., Yao, J. & Yang, Y. 2024 Designing turbulence with entangled vortices. *Proc. Natl. Acad. Sci. U.S.A.* **121**, e2405351121.

Yang, Y., Xiong, S. & Lu, Z. 2023 Applications of the vortex-surface field to flow visualization, modelling and simulation. *Flow* **3**, E33.

Zhou, L., Rauh, C. & Delgado, A. 2015 Multifractal-cascade model for inertial and dissipation ranges based on the wavelet reconstruction method. *Phys. Rev. E* **92**, 013010.